34th Annual International Conference of the IEEE EMBS
San Diego, California USA, 28 August - 1 September, 2012

Engineering of 7T transmit multi-row arrays

Mikhail Kozlov, Robert Turner, *Member, IEEE*

Abstract— **In evaluation of RF transmit array coils, realistic estimation of losses were included in simulations with the aim of obtaining a better match between experimental results and numerical predictions. This required customized design of lossy circuit components, to overcome the limitation of the available built-in capabilities of current simulation tools. Some of the more time-consuming post-processing stages were relocated into Matlab, speeding post-processing by up to a factor of 100. The resulting numerical data can support the fabrication of dual row array with as many as 8 elements in each row, and elements overlapped in the Z direction.**

I. Introduction

Experimental results for fabricated dual-row arrays (e.g. [1, 2]) and our initial numerical predictions [3, 4] differ in some aspects. Because it is becoming well understood that multi-row array design and fabrication are important in improvement in MRI performance of at high field, we focused our research on extending the capability of our numerical investigation approach. Our goals were: a) to investigate the effect of different losses on the performance of dual-row arrays; b) to explore the sensitivity of field homogeneity both to the ratio of transmit power delivered to each array row, and to the phase shift between rows.

II. Method

The fundamentals of the RF circuit and 3-D EM co-simulation work-flow, used for investigation of the geometry dependence of the performance of multi-row arrays, has been described in previous reports [3, 4, 5].

In our investigation [3, 4], the inductors forming part of the inductive decoupling networks were simulated as lossless, and individual losses of each lumped element were not analysed, because only built-in ADS circuit simulator components were used. To overcome this serious limitation of the available built-in capability of current simulation tools for investigation of the effect of different losses, we have designed customized lossy components to be used in ADS. Thus all components which represented lossy distributed capacitors, lossy decoupling networks (both for decoupling adjacent element inside array and for decoupling transmit only, receive only arrays), etc., were simulated with losses defined by vendors of these components, and loss data for each component were collected.

We analyzed quantities related to the power budget, obtained by direct calculation from volume and surface loss densities or wave quantities: a) $\boldsymbol{P}_{\mathbf{array\_refl}}$, the power reflected by the entire array; b) $\boldsymbol{P}_{\mathbf{radiated}}$ the radiated power; c) $\boldsymbol{P}_{\mathbf{array\_internal}}$, the inherent coil losses produced by lossy lumped elements (e.g. capacitors and inductors), dielectrics, and conductors; and d) $\boldsymbol{P}_{\mathbf{load}}$ the power absorbed by the entire load. Consistently with our previous reports, the same volumes of interest (**VOI**) were defined: $\mathbf{VOI_1}$ - the entire human brain, and $\mathbf{VOI_2}$ - the entire cerebellum. Array transmit properties were evaluated by considering the values of a) $\boldsymbol{B_1}+_{\mathbf{V}}$, the value of $\boldsymbol{B_1}+$ averaged over **VOI**, and its root-mean-square inhomogeneity ($\boldsymbol{IB_1}+_{\mathbf{V}}$ evaluated as a percentage "%"); b) $\boldsymbol{B_1}+_{\mathbf{s}}$, the mean $\boldsymbol{B_1}+$ averaged over the transverse central slice through the **VOI**, and its root-mean-square inhomogeneity ($\boldsymbol{IB_1}+_{\mathbf{s}}$ evaluated as a percentage "%"); c) $\boldsymbol{P}_{\mathbf{V}}$, the power deposited in the **VOI**; d) $\boldsymbol{E}_{\mathbf{V}}=\boldsymbol{B_1}+_{\mathbf{V}}/\sqrt{\boldsymbol{P}_{\mathbf{V}}}$, the **VOI** excitation efficiency; e) $\boldsymbol{SAR}_{\boldsymbol{10g}}$, the peak SAR averaged over 10 gram; f) $\boldsymbol{B}_{\boldsymbol{V\_sar}}=\boldsymbol{B_1}+_{\mathbf{V}}/\sqrt{\boldsymbol{SAR}_{\mathbf{10g}}}$, the safety excitation efficiency; g) $\xi_{\mathbf{v}}= \boldsymbol{B_1}+_{\mathbf{V}} / (\boldsymbol{B_1}+_{\mathbf{V}} + \boldsymbol{B_1}-_{\mathbf{V}})$, RF field polarization ratio averaged over both **VOI**s; and e) $\boldsymbol{B_1}+_{\mathbf{V}}/\sqrt{\boldsymbol{P}_{\mathbf{transmit}}}$, array transmit performance. Parameters also evaluated were $\boldsymbol{Q}_{\boldsymbol{load\_r1}}$ and $\boldsymbol{Q}_{\boldsymbol{load\_r2}}$, the quality factor for the first array element of the bottom and top rows respectively for circular polarization (CP) excitation mode, calculated at level -3dB from the frequency dependence of currents through correspondent array radiative elements; $\boldsymbol{maxS}_{\boldsymbol{21}}$, the maximum value of coupling between adjacent elements; $\boldsymbol{maxS}_{\boldsymbol{31}}$, the maximum value between the second adjacent elements; and $\boldsymbol{S}_{\boldsymbol{R21}}$, coupling between rows for given row excitation mode, calculated as $\sqrt{(\boldsymbol{P}_{\boldsymbol{row2\_refl}}/\boldsymbol{P}_{\boldsymbol{row1\_transmit}})}$, when only the first row was excited.

Although widely used for indirect evaluation of $\boldsymbol{P}_{\mathbf{array\_internal}}$ and $\boldsymbol{P}_{\mathbf{load}}$ [6], the $\boldsymbol{Q}_{\mathbf{load}}/\boldsymbol{Q}_{\mathbf{unload}}$ ratios are not tabulated here, since $\boldsymbol{P}_{\mathbf{array\_internal}}$ and $\boldsymbol{P}_{\mathbf{load}}$ were directly evaluated and also because the use of $\boldsymbol{Q}_{\mathbf{load}}/\boldsymbol{Q}_{\mathbf{unload}}$ can provide a misleading array power budget analysis at 300 MHz. The reasons for this are as follows: a) both for unloaded and loaded coils, radiation losses and the coupling between array elements differ significantly; b) the coupling between power supply and coil is altered by coil loading, which can invalidate the general requirement of critical coupling that enables calculation of the $\boldsymbol{Q}$-factor; and c) the reflected power $\boldsymbol{P}_{\mathbf{array\_refl}}$ is not taken into account. In our investigation $\boldsymbol{Q}_{\boldsymbol{load}}$ is used only for estimation of how large mismatch can be, due to imperfect tuning, between the array central operating frequency and the Larmor magnetic resonance frequency (F_{MRI}).

The capability limits have been reached for such up-to-date software packages as Agilent ADS 2011.10 (used as the RF circuit simulator), and Ansoft HFSS 14 (used as the 3-D EM tool) and use of a modern desktop computer (with 64 GB RAM) as regards the linear scaling of the numerical problem in the investigation of more and more complex array designs. For instance, the number of ports in the 3-D EM simulation domain must be kept below 128 to prevent the following primary post-processing problems: a) a significant and non-

M. Kozlov is with the Max Planck Institute for Human Cognitive and Brain Sciences, Leipzig, D-04103 Germany (corresponding author phone: +49-341-99402208; fax: +49-341-99402448; e-mail: kozlov@cbs.mpg.de).

R. Turner is with the Max Planck Institute for Human Cognitive and Brain Sciences, Leipzig, D-04103 Germany (e-mail: turner@cbs.mpg.de).

linear increase of field post-processing time; b) a significant and non-linear increase of circuit optimization time; c) the potential inconsistency of more than 100 GB of 3-D EM simulation data. The 3-D EM simulation data sets, which are significantly larger than available RAM, must be loaded piecewise for each HFSS post-processing step. Thus the HFSS post-processing can take longer than the computation of 3-D EM data by the HFSS solver. HFSS post-processing requires a very expensive HFSS front end license and hence the cost of using a large number of computers for post-processing can rapidly mount up.

8 and 4 (for 4 and 8 elements in one row respectively) distributed capacitors were placed in each radiative loop in our investigation [3, 4]. Two-row array fabrication experience has suggested that the number of distributed capacitors must be increased to obtain more stable array behavior at MRI scanner. Therefore in the current investigation the number of distributed capacitors in each element was increased to 16 and 12, for 4 and 8 elements in one row respectively. To keep the number of ports in the 3-D EM simulation domain below 128, some of the distributed capacitors were retained in 3-D EM domain, as shown on Fig.1.

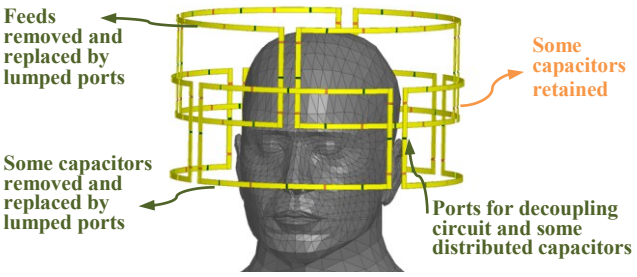

Figure 1. Actual 3D EM simulation setup.

A solution for speeding up 3-D EM post-processing consists in the following steps: a) to reduce the number of independent variables (dimension of 3-D EM data array) for electrical (***E***) and magnetic (***H***) fields to the number of array radiative elements, b) to calculate field related quantities using relatively inexpensive third party software tools with a powerful math library, for instance Matlab, c) to run the post-processing in a batch mode. Because HFSS field data is saved in files with proprietary formats, unsupported by other software tools, and there is no data link interface between Agilent ADS and HFSS, implementation of this solution was not a straightforward task, and some tradeoffs had to be considered.

We deduced the number of independent variables by exporting ***E*** and ***H*** fields (on an equidistant 1 mm mesh) from HFSS to temporary ASCII files, and then converted into files in Matlab format. Here the HFSS port powers were weighted by values calculated for individual excitation of each array radiative element. The field export time, which was originally about 30 minutes for each radiative element, was decreased by a factor of two by exporting field data only inside the human model included in numerical domain. An in-house Matlab procedure guided HFSS during data export and converted ASCII files into files in Matlab format.

Optimum excitation conditions were explored by running another Matlab procedure, which is about 100 times faster than HFSS post-processing, of the corresponding field-related quantities (e.g. $\boldsymbol{B_1}+_V$, $\boldsymbol{IB_1}+_V$). For each phase shift between rows (φ_{row}) in the range from 45° to 165°, the asymmetry in the power for excitation of each row $\boldsymbol{P_{asym}}$ ($\boldsymbol{P_{row1\_transmit}}= \boldsymbol{P_{transmit}}/2\cdot(1+ \boldsymbol{P_{asym}}/100)$ was swept in a range from -50 to 50. So far, elements in each row have been excited in circular polarization (CP) mode. For easy comparison of results, the entire array transmit power ($\boldsymbol{P_{transmit}}$) was always maintained at 8 W.

For the pairs of values of $\boldsymbol{P_{asym}}$ and φ_{row} resulting in nearly optimum values of $\boldsymbol{B_1}+_V$ and $\boldsymbol{IB_1}+_V$, the SAR-related quantities were obtained using an in-house calculation procedure which was reliable and relatively fast. This procedure utilized the Matlab Parallel Computing Toolbox™.

2D-losses (e.g. resistive losses in radiative elements) and 3D losses of thin objects (e.g. dielectric former) still have to be calculated in HFSS. Thus HFSS post-processing was used to obtain data for the entire power budget analysis for a set of optimal (from field homogeneity and safety excitation efficiency perspective) array excitation conditions.

To ensure that the array's field generation performance is optimal over the desired frequency range, variable electrical components connected to the array (for example trim capacitors) are adjusted until the RF fields are efficiently generated in a band around F_{MRI}. This procedure is commonly referred as the array optimization procedure, or array tuning. As with any other optimization procedure, MRI array tuning is guided by minimization of an error or cost function (*EF*), which is a measure of the difference between the actual and desired transmitter conditions.

In our previous reports [3, 4] two array optimization strategies were used. For the first strategy, which mimics commonly used optimization during fabrication, set of optimization criteria was defined (at the desired frequency F_{MRI}) as: a) the actual $\boldsymbol{S}_{xx}$ must be less than a target value $\boldsymbol{S}_{xx,Target}$, for each array element; b) the actual $\boldsymbol{S}_{xy}$ must be less than a target value $\boldsymbol{S}_{xy,Target}$, for each decoupled element pair. Hence

$$EF = \sum_{all\ array\ elements} w_{xx\_i} \times \left| S_{xx\_i} - S_{xx,Target} \right|^2 + \sum_{all\ decoupled\ pairs} w_{xy\_i} \times \left| S_{xy\_i} - S_{xy,Target} \right|^2 \quad (1)$$

where: $\boldsymbol{w}_{xx\_i}$ - weighting factor for the reflection coefficient $\boldsymbol{S}_{xx\_i}$ for the individual array element "***i***", $\boldsymbol{w}_{xy\_i}$- weighting factor for the reflection coefficient $\boldsymbol{S}_{xy\_i}$ for the "***i***" decoupled pair of array elements.

The second set consisted of a single criterion: for a specific excitation mode the power reflected by the entire array (i.e. $\boldsymbol{P}_{array\_refl}$) must be zero. Hence $\boldsymbol{EF}=|\boldsymbol{P}_{array\_refl}|^2$

For actual investigation we have added a third strategy (named as mode optimization), an extension of the previous two. This new optimization strategy was aimed at overcoming the major limitation of the strategies previously used: the unpredictable variation of transmit performance

(i.e. $B_1+_V/\sqrt{P_{transmit}}$) for different excitation modes. For a particular mode (or several modes), the power reflected by the entire array

$$P_{array\_refl} = a^H \times S^H \times S \times a \qquad (2)$$

(where S is the entire scattering matrix, a is the excitation vector, and subscript "^{H}" represents the complex conjugate transpose) can amount to a substantial fraction of $P_{transmit}$. This results in severe degradation of the transmit performance. A new EF is defined as

$$EF = \sum_{all\ array\ elements} w_{xx\_i} \times \left| S_{xx\_i} - S_{xx,Target} \right|^2 + \sum_{all\ decoupled\ pairs} w_{xy\_i} \times \left| S_{xy\_i} - S_{xy,Target} \right|^2 + \sum_{all\ modes} w_{m\_i} \times \left| P_{array\_refl\_i} \right|^2 \qquad (3)$$

(where: w_{m_i} are weighting factors for the reflected power of the entire multi-channel array for a given transmit mode "i", and $P_{array\_refl\_i}$ is the reflected power of the entire multi-channel array for a given transmit mode "i"). $P_{array\_refl\_i}$ was calculated for each mode using (2).

III. Results

We have extended our dual-row array simulation data base to more than 300 different array geometries. These geometries have been optimized using different definitions of lumped element loss, a range of decoupling techniques, and a variety of optimization strategies. Space limitations make it impossible to show all the results available. We focus on the most important findings and the relevant data for 280mm diameter array with one pin diode in each element, and with most practical lumped element loss definition: Q factor of all capacitors is equal 500, and Q factor of all inductor is equal 300, which correspond to Q factor of inductor made of 1 mm copper wire.

If the Q factor of the lumped elements is the same, increasing the number of distributed capacitors had no effect on field related properties in both CP and φ_{row}=+90° excitation modes for overlapped and non-overlapped dual row arrays. Field related properties of 2x4 and 2x8 ideally optimized arrays were similar in CP excitation mode, but B_{V1_sar} and E_{V1} were better for a 2x8 array in φ_{row}=+90° excitation mode, as shown in Table 1. Higher Q_{load} in φ_{row}=+90° mode (relative to CP mode) did not correspond to a decrease of $P_{array\_internal}$ or an increase of P_{load}, as discussed in [2]. On the contrary, $P_{array\_internal}$ increased and P_{load} decreased.

Adequate consideration of losses in the decoupling networks and capacitors can result in different conclusions for the suitability of a given dual-row array geometry for research and clinical applications. These losses have a significant influence on the second adjacent element coupling and S_{R21} (consequently on P_{array_refl}) and become dominant in high Q_{load} (high current) designs, which finally results in relative low $B_1+_V/\sqrt{P_{transmit}}$.

For a given array geometry, minimization of P_{array_refl} by mode optimization (for example) did not ensure a consequent proportional increase of power delivered to the volume of interest, because other power loss terms could significantly increase, and the power and B1+ could be concentrated in another sub-volume.

TABLE I. Overlap Array of 100mm Element Axial Lengh

Array design	*2x4 H100 8 capacitors*		*2x4 H100 16 capacitors*		*2x8 H100 4 capacitors*		*2x8 H100 12 capacitors*	
Excitation mode	*CP*	*+90*	*CP*	*+90*	*CP*	*+90*	*CP*	*+90*
B_1+_{V1}, μT	1.49	1.15	1.49	1.12	1.48	1.23	1.48	1.23
IB_1+_{V1}, %	24	17	24	17	24	13	24	13
B_1+_s, μT	1.69	1.12	1.68	1.08	1.7	1.28	1.68	1.28
IB_1+_s, %	20	13	19	13	19	9	19	9
P_{load}, W	6.09	5.59	6.15	5.64	6.02	4.74	6.02	4.75
P_{V1}, W	2.28	1.32	2.25	1.27	2.19	1.28	2.20	1.27
B_{V1_sar}, μT/√(W/kg)	0.73	0.57	0.73	0.56	0.75	0.75	0.75	0.75
E_{V1}, μT/√W	0.99	1.00	0.99	0.99	1.00	1.09	1.00	1.09
Q_{load_r1}	39	52	34	47	40	48	39	48
Q_{load_r2}	35	49	35	47	40	55	40	55
$P_{array\_internal}$	1.02	1.72	1.00	1.70	1.32	1.97	1.34	1.98

However, if the second array optimization step included adjusting P_{asym} or φ_{row}, or both, improvement of $B_1+_V/\sqrt{P_{transmit}}$ and IB_1+_V was obtained. This adjustment provided a flexible trade-off (increasing $B_1+_V/\sqrt{P_{transmit}}$ at the price of IB_1+_V deterioration and vice versa) for most of the geometries investigated.

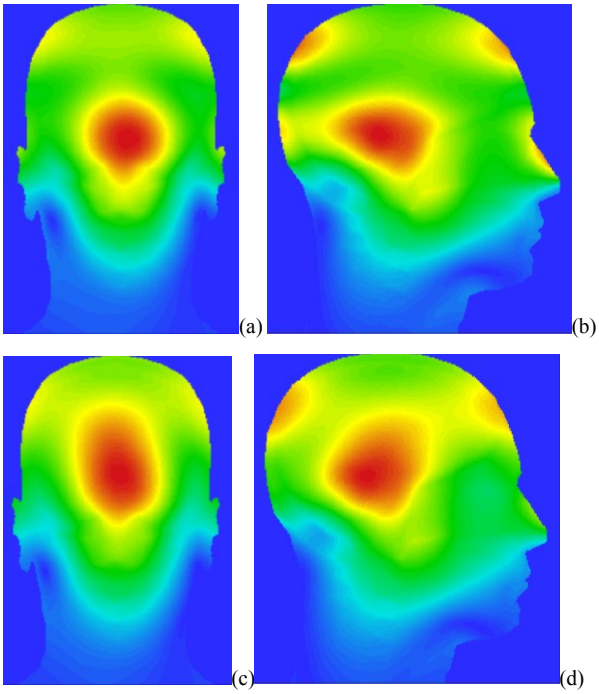

Figure 2. B_1+ slices rescaled to individual maximum, excitation mode φ_{row}=+90° : (a) and (b) – non-overlap array of 70mm element axial length, (c) and (d) overlap array of 100mm element axial length.

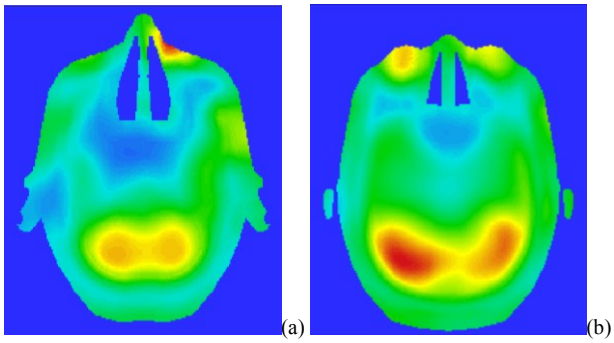

Figure 3. SAR_{10g} slices rescaled to individual maximum, excitation mode φ_{row}=+90° : (a) – non-overlap array of 70mm element axial length, (b) overlap array of 100mm element axial length.

Arrays with the same net Z direction length of 155 mm, having either 2x8 overlapped coils with 100 mm element length, or 2x8 non-overlapped 70 mm coils with element length, provided similar Z direction coverage and homogeneity over entire brain (Fig.2). However, both B_1+_V and B_{V_sar} were higher for the overlapped array. For the overlapped array B_{V_sar} was similar in CP and φ_{row}=+90 excitation modes, and varied slightly for all φ_{row} in the range from +45° to 165°. The SAR_{10g} was never higher than for CP excitation mode and the position of SAR_{10g} was stable inside the lower part of the head (Fig.3).

To achieve the best performance for optimization based on S parameters and P_{asym}=0 (the simplest experimental setup), the top and bottom rows of overlapped arrays were decoupled by very small inductors of 1…4 nH, in the numerical domain. Such low values could be impractical for actual coil fabrication. After mode optimization without row decoupling, these arrays provided similar performance to decoupled arrays if P_{asym} was in the range from -45 to 15. An example is shown in Fig.4 and Fig.5.

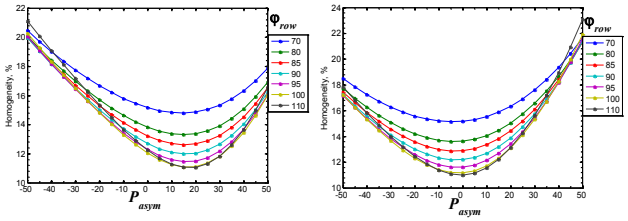

Figure 4. Dependence of IB_1+_{V1} on φ_{row} and the asymmetry in the power for excitation of each row. Left: 2x8 H100 12 capacitors array, right: 2x8 H100 12 capacitors array with 2nH decoupling inductiors

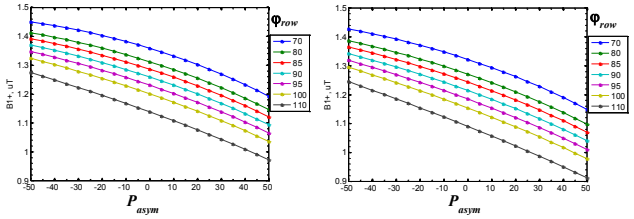

Figure 5. Dependence of B_1+_{V1} on φ_{row} and the asymmetry in the power for excitation of each row. Left: 2x8 H100 12 capacitors array, right: 2x8 H100 12 capacitors array with 2nH decoupling inductiors

We found that mode optimization in conjunction with adjustment of P_{asym} was a powerful tool for getting close to the best transmit performance, together with relatively small S_{R21} (~-15db), for 2x8 overlap array, although this optimization resulted in a relatively high $maxS_{11}$ (~-13db), $maxS_{21}$ (~-10db) and $maxS_{31}$ (~-10db).

For a non-overlapped array, rotation of the top row relative to the bottom row resulted in similar performance and homogeneity, if P_{asym} and φ_{row} were properly adjusted. The best performance for non-overlapped arrays was found when P_{asym} was in the range from -30 to -10.

IV. Discussion

The number of distributed capacitors had no influence on the array transmit performance, because neither RF cable traps nor coax cable interconnection wiring have yet been included in the simulation domain (ideal common-mode-current suppression assumption). To obtain the general dependence of array performance versus array element spatial distribution, it helps to use a smaller number of distributed capacitors, because all distributed capacitors can be substituted by ports (no prediction of distributed capacitor values are required).Thus a) different decoupling strategies and b) array properties for different level of distributed capacitor losses can be analyzed on the basis of only one 3D-EM simulation.

The preliminary simulation data (in term of actual fabricated array distributed capacitor topology) were important for correct prediction of values for distributed capacitors retained in 3D-EM domain during the final array design investigation. For these final simulations, the losses of the distributed capacitors were determined from the relevant vendor datasheets. The modeled components developed for RF circuit simulation provide good potential for reverse engineering of networks for decoupling adjacent elements, adjacent rows, and transmit-only receive-only coil.

The results derived from sophisticated static RF shimming optimization of arbitrary transmit amplitudes and phases, as well as calculation of transmit SENSE pulses and worst case SAR analysis, should be performed before final decisions regarding coil configuration are made.

References

[1] G. Shajan, J. Hoffmann, K. Scheffler, and Rolf Pohmann, "A 16-Element Dual-row Transmit Coil Array for 3D RF Shimming at 9.4 T," Proceedings of the 20th Annual Meeting, Melbourne, Australia, p. 3831, May 2012.

[2] K. Gilbert, JG. Belliveau, A. Curtis, J. Gati, L. Klassen, and R. Menon, "A Conformal Transceive Array for 7-T Neuroimaging," Magnetic Resonance in Medicine, July 7 2011 [Epub ahead of print]

[3] M. Kozlov, R. Turner, "Analysis of RF transmit performance for a multi-row multi-channel MRI loop array at 300 and 400 MHz," Proceedings of the Asia-Pacific Microwave Conference 2011, Melbourne, Australia, p. 1190-1193, December 2011.

[4] M. Kozlov, R. Turner: " Analysis of RF transmit performance for a 7T dual row multichannel MRI loop array," Proceedings of 33rd Annual International Conference of the IEEE EMBS, Boston, USA, p. 547-553, August 2011.

[5] M. Vogel, R. Kleihorst: "Large-Scale Simulations Including a Human-Body Model for MRI," Proceedings of IEEE Microwave Conference 2007, p. 1345-1348.

[6] R. Lemdiasov , A. Obi, R. Ludwig, "A numerical postprocessing procedure for analyzing radio frequency MRI coils," *Concepts in Magnetic Resonance Part A,* Vol. 38A(4), 133–147, 2011.